Biaxial Testing of High Strength Fiber Composite Cylinders for Pulsed Magnet Reinforcement

Bednar, N., NHMFL/FAMU-FSU College of Engineering, and Center for Materials Research and Technology
Garmestani, H., NHMFL/FAMU-FSU COE and MARTECH

A program of research has been initiated to investigate the biaxial mechanical properties of carbon fiber reinforced composite cylinders under axial compression and hoop tension. The understanding of the failure mechanisms of these composites under biaxial loads is extremely important in the design of pulsed magnets. These composites are used as reinforcements for both the inner conducting layers and as an overall exterior reinforcement. Testing of actual pulsed magnets to ascertain design change effects of composite reinforcement schemes on maximum attainable field can be expensive. A standard biaxial testing method is desirable that is specific to the design of pulsed magnets. In this investigation an attempt is made to produce a standard testing procedure aimed at measuring the biaxial mechanical properties (elastic, plastic, and failure envelope) of composite materials. This methodology was applied to two different carbon-based composites. The results of these tests are compared to theoretical predictions, specifically those due to Tsai Wu.

The composite specimens were considered as thin wall pressure vessels with a wall thickness of 1 mm and an internal diameter of 38.1 mm. The specimen is a hoop wound composite with reinforced ends. Overall length of each specimen was 152 mm. Each end has a 12.7 mm thick G-10 fiberglass endcap with annular channel 6.35 mm deep. The specimen end was inserted into the channel and secured with two-part epoxy. Each endcap had a threaded oil inlet and air release port into which a 3.53 mm brass bushing was threaded and epoxied. A critical component of the specimen design also included a flexible polyurethane internal bladder which was cast from liquid form onto the inside wall of the specimen. A 22 kip MTS servo-hydraulic machine and an Enerpac hand pump, which delivered a maximum of 10 ksi were used to provide a biaxial state of stress.

Two different kinds of carbon fiber composite specimens were tested. The first group was manufactured at the NHMFL using a wet winding technique. The carbon fibers in this group were Hercules Magnamite IM8 and the epoxy matrix was CTD 521. The second group of specimens tested were purchased from SpyroTech Inc. of Lincoln, Nebraska. The fibers used for these samples were Voltek Panex carbon fibers and the epoxy matrix used was Shell 9405-9470. The cure cycle was 82 °C for 4 hours, then 121 °C for another 4 hours. The cure cycle for the NHMFL specimens was 90 °C for approximately 8 hours.

Figure 1 shows a graphic representation of the failure points for applicable specimens. A failure criteria developed by Tsai Wu in the following form was used to compare the results

$$f(\sigma_i) = F_i \sigma_i + F_{ij} \sigma_i \sigma_j = 1 \qquad (1)$$

where terms higher than second order are omitted. In general the results show that only three parameters of the model are needed for a complete characterization of the failure surfaces. The comparison shows that such a model may be sufficient to characterize the failure history in these two materials. The biaxial fixture design here shows good promise in standardization of such tests to provide a reproducible set of data for biaxial experiments.

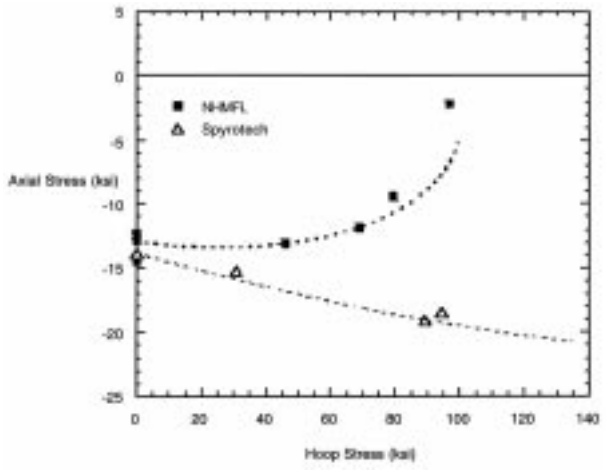

Figure 1. Experimental data and comparison to Tsai Wu's analysis for the two types of materials.

Effect of Deformation Mode on the Properties of Cu-Base Conductor Wires

Brandao, L.P.M., NHMFL and Instituto Militar de Engenharia, Rio de Janeiro, Brazil
Kalu, P.N., FAMU-FSU College of Engineering

One of the principal requirements for a good conductor material used in high-field pulsed magnets is high mechanical strength. Of the three known methods for strengthening alloys, the combination of precipitation hardening and work-hardening have been shown to exhibit the best properties. In order to obtain the necessary level of work hardening, heavy deformation is required. Such heavy deformation can be accomplished through wire drawing, swaging or a combination of the two methods. Texture development in such heavily deformed materials is of vital interest because the strength of material is affected by texture, and texture in turn is very sensitive to the deformation process.[1,2]

In this study, the effect of the mode of fabrication on texture development is presented. Three Cu-Nb/Ti composites were deformed to a strain of 95% via (a) swaging, (b) drawing and (c) a combination of both methods. There was a significant difference in the texture resulting from these three modes of deformation. The swaged material exhibited strong texture with a predominance of copper, Cu {112}<111>, Goss, G {110}<001>, and {110}<111> components. The drawn material showed a similar texture but with less intensity. However, the swaged plus drawn material exhibited random texture with a maximum intensity level of 1.5x random. A correlation has been made between the strength of the materials and the texture developed.

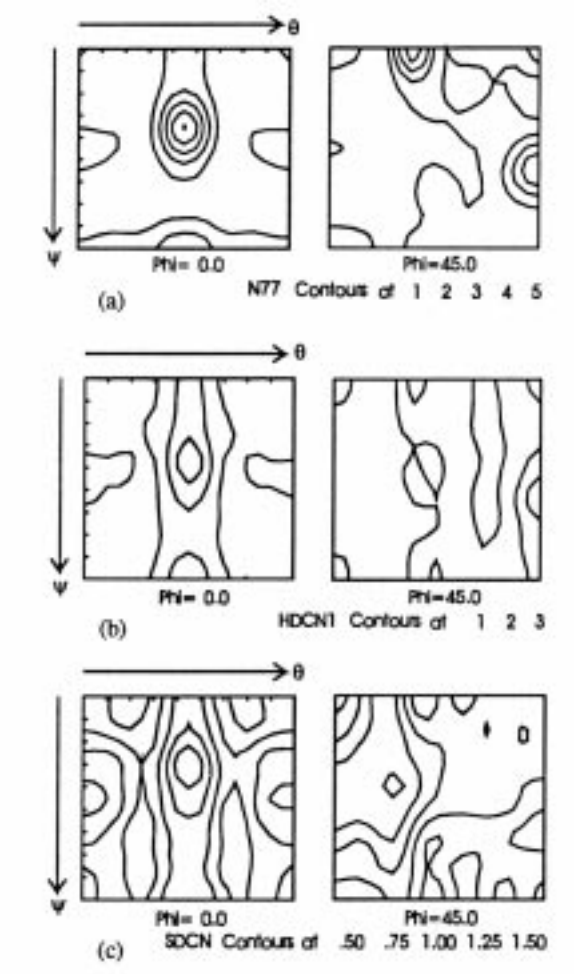

Figure 1. ODF sections for the Cu-Nb/Ti composite wires at the conclusion of processing for (a) swaged, (b) drawn and (c) swaged plus drawn.

References:

1 Canova, G.R., *et al.*, *The Development of Deformation Texture and Resulting Properties of FCC Materials, ICOTOM 6*, eds. C.M. Brakman, *et al.*, Netherlands Soc. Mater. Sci., 573 (1984).
2 Canova, G.R., *et al.*, J. Mech. Phys. Sol., 33, 371 (1985).

Characterization of Copper-Stainless Steel, External Reinforcement of the 900 MHz NMR Magnet

Dixon, I.R., NHMFL
Markiewicz, W.D., NHMFL
Walsh, R.P., NHMFL

Summary. The external reinforcement of the 900 MHz NMR magnet is composed of a 316L stainless steel core with a high purity copper jacket and a glass braid insulation. During the insulation process a short in-line anneal is required. The implications on the yield strength from the anneal are examined by measuring the mechanical properties. Tests are performed at room temperature and at 4.2 K. Results are compared with values in the literature.

Mechanical Measurements. A total of three samples were measured at NHMFL. One tested at room temperature and two at 4.2 K. The dimensions of the wires are 1.6 mm x 2.8 mm with nominally 12% copper. Thus the cross-sectional area of the wire is 4.415 mm^2 and of the stainless steel is 3.885 mm^2 taking into account a 0.275 mm corner radius.

The primary results of interest of the tests are the yield point and Young's modulus. A wire extensometer was used to measure deformation of the samples. The stress-strain curve at room temperature of the first sample is shown in Figure 1. The sample was loaded until it yielded where the load was then cycled. The modulus was measured to be 160 GPa and the yield was 362 MPa at a 0.2% offset.

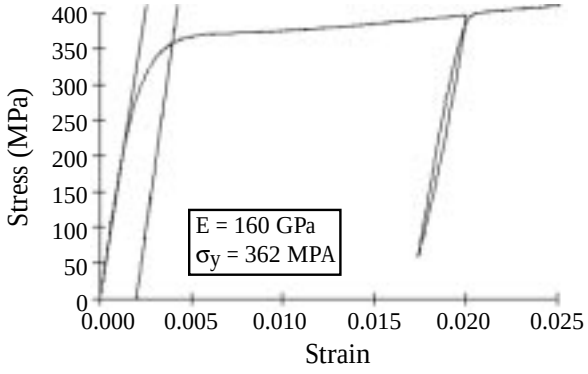

Figure 1. Stress-strain curve of annealed copper-stainless steel at 297 K, Sample 1.

The two annealed samples tested at 4.2 K are shown in Figure 2. A little variability exist in the results but behave very similarly. The moduli are 181.7 GPa and 189.1 GPa and the yield points are 804.4 MPa and 792.7 MPa. The differences between the measured moduli may be attributed to the straightness of the samples. Discontinuous yielding is shown to be present in the two tests by the short drops in the stress-strain curves. The samples were not pulled to failure.

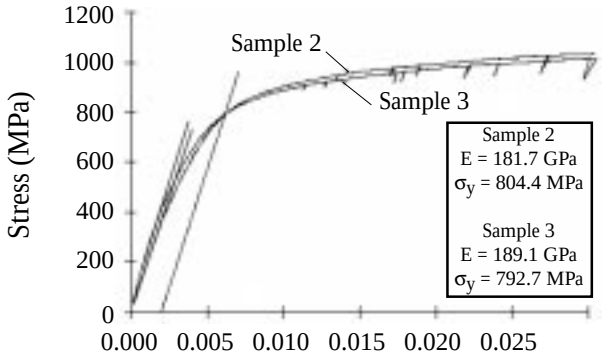

Figure 2. Stress-strain curve of annealed copper-stainless steel at 4.2 K, Samples 2 and 3.

Data of fully annealed steel is comparable to the measurements from scaling the results by the fraction of steel. Assuming that the copper does not contribute to the stiffness and strength measurements, a modulus of 182 GPa and a yield of 818 MPa results. This is summarized in Table 1. Thus the external reinforcement is shown to see a full anneal during the insulation process.

Table 1. Summary of copper-stainless steel mechanical properties.

Sample	Temp. (K)	Modulus (GPa)	Yield (MPa)
Sample 1	297	160	362
Sample 2	4.2	181.7	804.4
Sample 3	4.2	189.1	792.7
Full Anneal	4.2	182	818

Critical Current Measurements of NbTi Superconductor #110 at Temperatures of 4.2 K and 1.8 K

Dixon, I.R., NHMFL
Markiewicz, W.D., NHMFL
Pickard, K.P., NHMFL

Introduction. Critical current tests are performed on NbTi superconductor for the primary purpose of determining the n-value characteristics over a range of fields and temperatures. The superconductor, inventoried as #110, is a round wire, 1.4 mm in diameter, with a copper to superconductor ratio of 4.2.

The tests were performed in the resistive magnet user facility at NHMFL. The results presented give critical current values defined when the sample voltage exceeds 0.1 μV/cm and 1.0 μV/cm above the baseline voltage. Voltage taps are placed over a span of three conductor turns, creating a 28 cm sample length. The sample was mounted on a sample holder, soldered across a Ti-6Al-4V shunt.

Results. The superconductor was tested at 4.2 K and 1.8 K. The current-voltage traces are plotted in Figure 1 for the 4.2 K measurements. With a baseline voltage of 2.1 μV, the superconducting transitions are defined at 4.9 μV and 30.1 μV. A summary of the critical currents and current densities are listed in Table 1 at 4.2 K and Table 2 at 1.8 K.

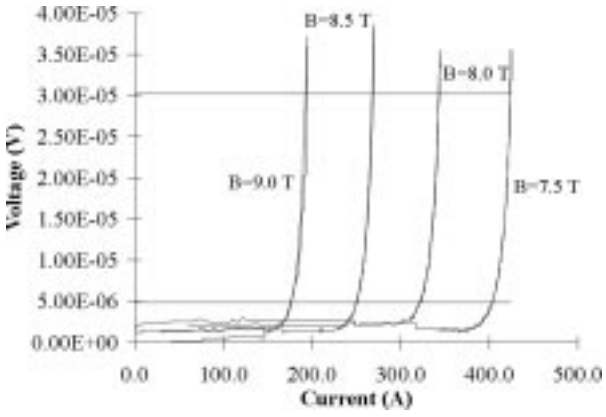

Figure 1. Superconducting transition of NbTi #110 at various fields and at 4.2 K.

Table 1. Critical current densities of NbTi superconductor #110, tested at 4.2 K.

	0.1 μV/cm Above Baseline		1.0 μV/cm Above Baseline	
B (T)	I_c (A)	J_c (A/mm²)	I_c (A)	J_c (A/mm²)
7.5	403.95	1402.86	424.33	1473.65
8.0	324.17	1125.80	343.95	1194.51
8.5	248.90	864.40	268.67	933.05
9.0	182.86	635.04	195.05	677.37

Table 2. Critical current densities of NbTi superconductor #110, tested at 1.8 K.

	0.1 μV/cm Above Baseline		1.0 μV/cm Above Baseline	
B (T)	I_c (A)	J_c (A/mm²)	I_c (A)	J_c (A/mm²)
9.0	673.95	2340.52	699.03	2427.64
9.5	594.83	2065.77	620.16	2153.74
10.0	518.94	1802.20	540.35	1876.58
10.5	438.73	1523.63	459.49	1595.74

The B_{c2} is 10.2 T and 13.3 T at 4.2 K and 1.8 K respectively. The n-value is computed to quantify the sharpness of the superconducting transition by fitting a polynomial through the data in the form $V = cI^n$. The n-values are listed in Table 3. The n-values behave linearly with field, except for the 10.5 T data point at 1.8 K which drops off. A direct shift between temperatures is not shown to occur, rather the slope decreases at lower temperature.

Table 3. N-values of NbTi #110.

B (T)	N-Value T = 4.2 K	B (T)	N-Value T = 1.8 K
7.5	46.35	9.0	57.16
8.0	37.24	9.5	56.47
8.5	29.77	10.0	54.90
9.0	22.50	10.5	49.89

Microtexture Characterization of LD-MOCVD Processed Thin Film Materials Exhibiting Giant Magnetoresistance

Garmestani, H., FAMU-FSU College of Engineering/ NHMFL/Center for Materials Research and Technology/ Center for Nonlinear and Nonequilibrium Aeroscience
Dahmen, K.H., FSU, Chemistry and MARTECH
Brandao, L.P.M., FAMU-FSU COE/NHMFL/ MARTECH/CeNNAS
Weaver, M.L., FAMU-FSU COE/NHMFL/ MARTECH/CeNNAS
Gillman, E.S., FSU, Chemistry and MARTECH

Thin films of $La_{1-x}Ca_xMnO_3$ (LCMO) have been produced on (001) oriented $LaAlO_3$ (LAO) and yttrium stabilized zirconia (YSZ) substrates by liquid delivery metal organic chemical vapor deposition (LD-MOCVD). XRD analyses showed that the films were epitaxially grown on LAO substrates and were monocrystalline at thickness of less than 500 Å. At thickness of greater than 500 Å, the films became polycrystalline but maintained their high orientation. Films grown on YSZ were always polycrystalline but were also highly oriented. Regardless of the substrate, the 1500 Å thick polycrystalline films exhibited substantially significant magnetoresistance ratios even above room temperature.

Epitaxially grown thin films have been shown to exhibit "colossal magnetoresistance" near the Curie temperature (T_c). Thin films of these materials are being considered in applications such as electrochemical and magnetic sensors and as potential replacements for GMR read heads in the magnetic recording industry. To achieve such goals, however, it will be necessary to develop economical methods to produce thin films exhibiting optimal magnetic and electronic properties. Recently, Dahmen and coworkers[1,2] have reported success in the growth of epitaxial thin films using a liquid delivery metal organic chemical vapor deposition (LD-MOCVD) technique. In view of the increasing importance of these films in a variety of technological applications, an investigation has been initiated of thin film oxides deposited on single-crystal substrates by the LD-MOCVD process.

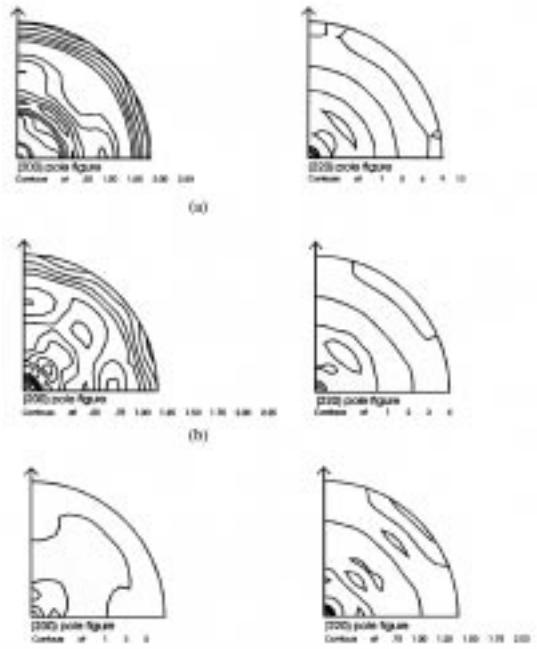

Figure 1. (100) and (110) pole figures for LCMO deposited on YSZ. (a) 500 Å thickness, (b) 1000 Å thickness, and (c) 1500 Å thickness.

Thin films of lanthanum manganites were prepared on (001) oriented yttrium stabilized zirconia (YSZ), and $LaAlO_3$ (LAO) under reaction conditions designed to optimize T_c and magnetotransport properties. Incomplete pole figures were obtained using the reflection technique described by Schultz. The resulting data was analyzed via the spherical harmonics method using the popLA software package from which the complete pole figures were re-constructed using the spherical harmonics approach. Texture variations of the LCMO films on LAO are summarized in the pole figures shown in Figure 1.

The crystalographic texture can be correlated with the magnetoresistive response seen in these films. X-ray diffraction and pole figure measurements indicate that films grown on LAO are epitaxial and exhibit a high degree of preferred (001) orientation. Resistivity and magnetoresistivity is sharply peaked in the vicinity of T_c in these films. X-ray diffraction and pole figure measurements of LCMO thin films on YSZ show a preferred (110) orientation. These films show a substantial greater resistance than the films on LAO and a large MR response which is nearly constant well below T_c. These results demonstrated that by taking advantage of the dependence of texture on substrates the MR response in these films can be controlled.

Acknowledgment. The authors acknowledge support under grant ONR-N0001496-1-0767.

References:

1 Gillman, E.S., *et al.*, in *Chemical Vapor Deposition-Proceedings of the Fourteenth International Conference and EUROCVD-11*, eds. M.D. Allendorf, *et al*., The Electrochemical Society, NJ, 1506 (1997).

2 Dahmen, K.-H., *et al*., *Chemical Vapor Deposition (Advanced Materials)*, 3, 27-30 (1997).

Development of Materials Related to the 60 T and 100 T Magnets

Han, K., LANL
Embury, J.D., LANL

In the past year, the effort in materials science related to the 60 T and 100 T magnets at Los Alamos has been concentrated in three areas: (a) development of a fabrication route for Cu-Ag wire in collaboration with Handy and Harman and IGC; (b) investigation of the mechanical properties of a variety of potential high strength high conductivity materials; and (c) selection of the reinforcement materials for the coils and development of a fabrication route for these materials. The selection of the conductors and reinforcement materials is based on their mechanical properties and electrical properties at liquid nitrogen temperature (77 K). We have taken the approach of trying to relate the properties both to design requirements and to the service life of magnet. Thus, we have given some consideration both to the role of the internal stresses developed during the fabrication on the elastic-plastic transition and on the mechanical and thermal stability of heavily drawn wires. The feasibility of the fabrication route and the cost of manufacturing the materials must also be considered. We have emphasized the need to develop a fabrication route capable of producing the conductors with homogeneous mechanical and electrical properties and with a cross-section of 8.6 mm x 5.2 mm and 146 m in length or longer for a 100 T magnet. After optimization of the fabrication routes, we have produced 8.6 mm x 5.2 mm x 1.6 mm corner radius Cu-Ag materials with a flow stress at -196 ˚C larger than 1 GPa at a true strain $\varepsilon = 0.002$. We are planning to produce longer lengths of wire using the optimized fabrication route.

GlidCop Al-15 and Al-60 are produced by internal oxidization of the Cu-Al powder, extrusion and cold drawing. The final wire sizes are 5.2 mm x 8.6 mm x 1.6 corner radius, 6.7 mm x 11 mm x 1.6 corner radius and 7.5 mm x 12.5 mm x 1.6 corner radius. These materials have been tested and are currently being used in the 60 T magnet.

Cyclic softening, which is the strength decrease due to the fatigue, was investigated using mainly Cu-Ag, GlidCop Al-15 and GlidCop Al-60 in the cold rolled and drawn conditions. The fatigue test results in liquid nitrogen showed less cyclic softening than at room temperature. In all the experimental conditions, the rounding of the stress-strain curve resulting from internal stresses was less prominent after the fatigue test. The internal stresses are thought to be due both to the non-uniformity of the deformation and compatibility of two phases in co-deformation. For the magnet design, the materials are strained essentially in the elastic range. Therefore, it appears that the contribution of the internal stress to the strain-stress curve can be diminished by stretching the materials by a small additional tensile strain, by reverse bending or by low temperature thermal cycles and this may be of value in optimizing of the overall production route and fabrication of the magnet.

The reinforcement vessel can be considered as a pressure vessel operating at 77 K. The materials for the reinforcement should have sufficient stiffness, strength, and toughness for the service requirements. We have compared the Young's modulus, yield stress, and fracture toughness of different cryogenic materials that can be used as reinforcement materials.

The survey was first conducted by selection of suitable candidate materials with good cryogenic properties. Six materials have been considered: maraging steel C250, maraging steel C300, Inconel 718, Nitronic-40, MP35N, and Elgiloy. Due to the larger sizes (cylinders as large as 1.1 m in diameter) of the reinforcement materials, the materials with different geometries have been fabricated and tested in order to measure the tensile strength, fracture toughness, and thermal expansion. In addition, the cylinders with and without holes have been tested to simulate the mechanical behavior at the cryogenic conditions in structures containing defects.

Electrical and Thermal Resistivity of Eutectic Ag-Cu

Heringhaus, F., NHMFL and RWTH Aachen, Germany
Gottstein, G., RWTH Aachen, Germany
Schneider-Muntau, H.-J., NHMFL

The relationship of electrical and thermal resistivity provides information on the scattering mechanisms and, in the latter case, the ratio of the electronic and phononic contributions. Both resistivities were measured by means of a steady-state method in longitudinal flow along the wire axis between 295 K and 30 K. The specimens were wire-deformed, eutectic Ag-Cu with degrees of deformation up to η=8. Their lamellar as-cast microstructure refines during deformation, leading to strong changes in the macroscopic properties.

From Figure 1 becomes apparent that plastic deformation leads to higher resistivities, electrical and thermal, at all temperatures. Decreasing temperature leads to a decrease in electrical resistivity and an increase in thermal resistivity. In the former case, this is in agreement with the behavior of the pure elements Ag and Cu; in the latter case it contradicts the behavior of the pure elements. Both properties reveal increasing deviations from the rule of mixture values with decreasing temperatures, which amount to about 400% for the electrical resistivity and almost 1400% for the thermal resistivity at η=8 and 30 K. This behavior is due to the "size effect" as well as mutual solution. For the thermal resistivity, the development of a strong anisotropy in the phonon mean free path, which may occur in the interface layers,[1] provides an additional contribution.

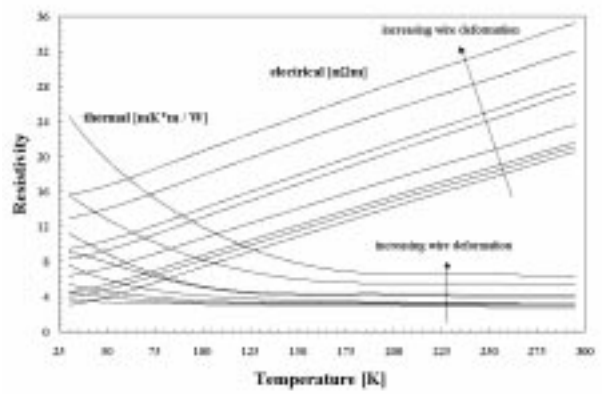

Figure 1. Electrical and thermal resistivity of eutectic Ag-Cu.

The data presented was used for an analysis of the Lorenz number as a function of temperature. This analysis revealed a minimum in the Lorenz number, the value of which is presented in Figure 2 as a function of the wire deformation. The strong decrease in the minimum values indicates that the electronic contribution to the thermal conductivity is not dominant anymore in highly deformed eutectic composites, as is typically found in metallic conductors.

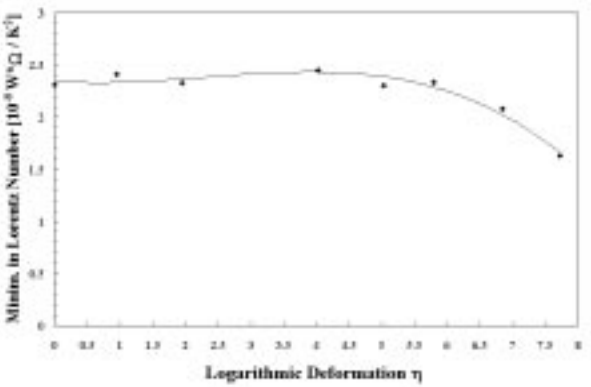

Figure 2. Minimum of the Lorenz number of Ag-Cu.

References:

1 Ziman, J.M., *Electrons and Phonons*, Clarendon Press, (1967).

Optimization Methodology for High Strength Conductors

Heringhaus, F., NHMFL and IMM, RWTH Aachen, Germany
Prestemon, S.O., NHMFL
Gottstein, G., RWTH Aachen, Germany
Schneider-Muntau, H.-J., NHMFL

A mathematical notion is described and applied that allows for the determination of the optimum microstructure for any given combination of any given number of properties. First, each property, P, is normalized to its rule of mixture (ROM) value,

P_{ROM}, and analytically expressed as a function of the microstructure, e.g., the lamella thickness, LT. The normalization ensures that only the microstructural effects are taken into account and that scaling effects are prevented. Then, the analytic expressions for the normalized properties, $\tilde{P}$, are differentiated and the ratio of the derivatives, $k_{i,j}$, is determined. An optimum combination of the two properties, P_i and P_j, for a desired ratio of their derivatives is achieved at a lamella thickness where Eqn. 1 is fulfilled.

$$\frac{d\tilde{P}_i}{d\tilde{P}_j} - k_{i,j} = 0 \qquad (1)$$

When more than one set of properties is involved, the resulting set of equations of the form Eqn. 1 will not be satisfied simultaneously. A minimization is therefore performed, where each set of properties is given a relative weight, $m_{i,j}$. This minimization procedure can then be applied to the cost function C(LT) in Eqn. 2, where n is the number of properties to be combined. Note that this formulation also applies to the case of only one combination of properties as in Eqn. 1 and in fact generalizes that equation for all values of $k_{i,j}$. In other words, while Eqn. 1 can only be satisfied for a judicious choice of values $k_{i,j}$, a minimization of Eqn. 2 will always find the best possible lamella thickness for the chosen parameters.

$$C\ (\mathrm{LT}) = \sum_{i=1,j>i}^{n-1} \left[m_{i,j} \cdot \left(\frac{d\tilde{P}_i}{d\tilde{P}_j} - k_{i,j} \right)^2 \right] \qquad (2)$$

The derivatives of the normalized ultimate tensile strength, UTS, and electrical resistivity, ρ, as a function of LT for T = 77 K intersect at LT = 16.5 nm (Figure 1). For a derivative ratio of $k_{i,j} = 1$, this constitutes the optimum LT for combinations of high UTS and low ρ. A numeric minimization of Eqn. 2 was carried out for a combination of UTS, ρ , and thermal resistivity, W, at T = 77 K. Figure 2 gives the results of the optimum LT in a three-dimensional view as a function of the relative weight of their respective ratios. The weight factors are m_1 for a combination of UTS and ρ, m_2 for UTS and W, and m_3 for ρ and W. All $k_{i,j}$ are unity. The optimum lamella thickness of LT = 16.5 nm for the combination of UTS and ρ only, can be found again at $m_2/m_1 = m_3/m_1 = 0$. This optimum increases with any increase in weight factor of one or more combinations of properties, representing the contradiction in the mechanisms that determine the dependence of these properties on the microstructure. Any non-trivial solution of Eqn. 2 for more than one combination of properties, i.e., more than two properties, will lead to a minimum of *C*(LT) greater than zero. The value of C_{min} can thus be reviewed as quantifying the inherent contradictions in the desired properties.

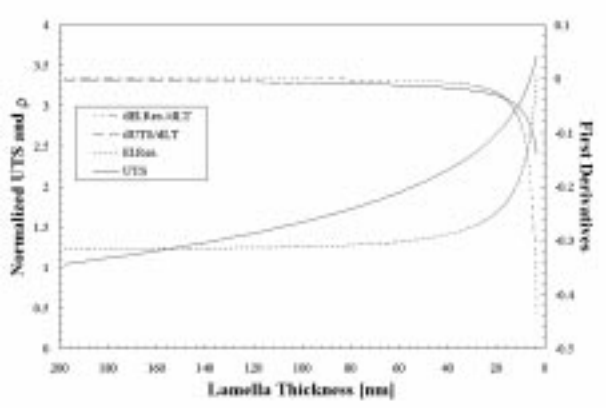

Figure 1. Normalized ultimate tensile strength (UTS) and electrical resistivity ρ of Ag-Cu at T = 77 K.

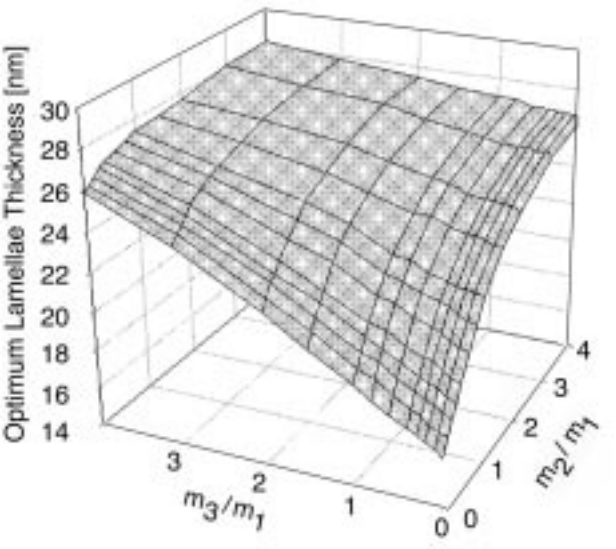

Figure 2. Optimum LT for combinations of UTS, ρ, and W at T = 77 K.

References:

1 Heringhaus, F., *et al*., Advances in Cryogenic Engineering, in press.

Texture Evolution and Strength in Cu, Ag, and Ag-Cu

Heringhaus, F., NHMFL and IMM, RWTH Aachen, Germany
Gottstein, G., RWTH Aachen, Germany
Schneider-Muntau, H.-J., NHMFL

The Taylor theory of polycrystal deformation[1] describes the relationship between the crystallographic texture of metals and their mechanical strength. The major elements are the resolved shear stress on the slip systems and the strain compatibility at the grain-boundaries that necessitates the activation of five independent slip systems. The change in strength caused by a change in crystallographic texture scales with the ratio of the Taylor factors, M, of these textures. In face-center cubic (fcc) metals, the development of textures with the highest Taylor factors (<111> and <110>) allows for a maximum increase in strength of approximately 20%.[2]

An experimental investigation is presented that compares the strengthening due to texture evolution of pure Ag, pure Cu, and eutectic Ag-Cu as it occurs during wire deformation.

The macrotexture development was investigated by means of an automated x-ray goniometer[3] that was employed to measure pole figures in the back reflection mode.[4] The results are presented in inverse pole figures in intensity factors, I, of the random distribution with respect to the wire axis.

Figure 1 gives the inverse pole figures of Ag, Cu, Ag in Ag-Cu, and Cu in Ag-Cu after heavy wire deformation. Ag and Cu show a dual fiber texture with strong intensities on <100> and <111> as is typical for fcc metals after uniaxial deformation and in accord with the Taylor theory. The maxima are located on opposite fibers, namely <100> for Ag and <111> for Cu, which may be explained by their difference in stacking fault energy. Both phases of the eutectic develop strong single fiber textures in <111>. This is in contradiction to the findings

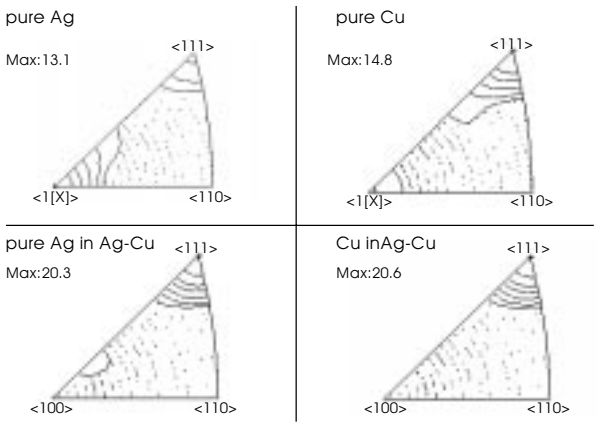

Figure 1. Inverse pole figures of heavily deformed pure Ag, pure Cu, Ag in Ag-Cu, and Cu in Ag-Cu.

in the bulk, pure phases, however, the mechanisms of plastic flow and dislocation interaction in fine scale composites such a eutectic Ag-Cu are only poorly understood and may be very different from the bulk.

The average Taylor factors, M, of these four textures were determined by a full-constraints Taylor simulation step with η=0.01% strain following a discretization of the macrotexture. For pure Ag, M=2.70 and for pure Cu, M=3.35 were found. An investigation of the average Taylor factor of the phases of the eutectic as a function of the wire deformation revealed an increase from about M=3.09 (as-cast) to M=3.42 for Ag and M=3.47 for Cu. While the as-cast values are very close to M=3.06 (random texture), the average Taylor factors of the <111> textures are still significantly away from M=3.67 (perfect <111> fiber texture). The changes in strength of an fcc metal with development of a texture other than random scale with M/3.06. It becomes apparent that the texture evolution weakens pure Ag, while it strengthens pure Cu and both phases of the eutectic. All increases in strength, however, are still considerably apart from the maximum of 20%. Furthermore, while the texture evolution in pure Ag and Cu may be held accountable for their work-hardening, it fails to explain the strong increase in strength that is observed in the eutectic Ag-Cu (Figure 2).

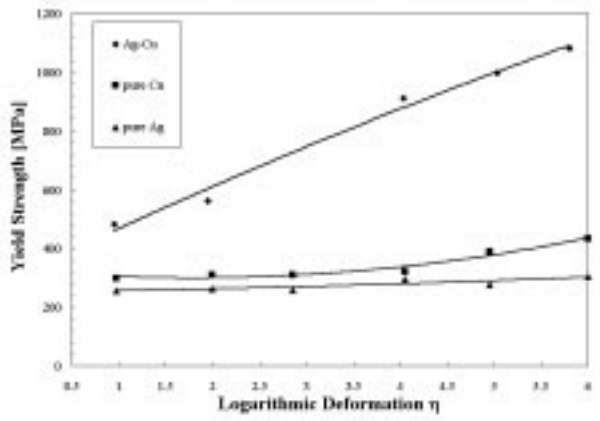

Figure 2. Tensile yield strength of pure Ag, pure Cu, and eutectic Ag-Cu.

References:

1 Taylor, G.I., Journal of Inst. Met., 62, 307-324 (1938).
2 Hosford, W.F. *The Mechanics of Crystals and Textured Polycrystals*, Oxford University Press, (1993).
3 Hirsch, J., *et al*., ICOTOM 8, 765-776, (1984).
4 Schulz, L.G., J. of Appl. Phys., 20, 1030-1036 (1949).

Development and Characterization of Cu-Base Conductor Wires for Pulsed Magnets

Kalu, P.N., FAMU/FSU College of Engineering
Brandao, L.P.M., NHMFL and Instituto Militar de Engenharia, Rio de Janeiro, Brazil
Heringhaus, F., NHMFL and IMM, RWTH Aachen, Germany

Environmental scanning electron microscopy (ESEM) has been used to monitor the evolution of microstructure in swaged, drawn and swaged plus drawn Cu-Ag and Cu-Nb/Ti composite. The main objective of the project is to understand the metallurgical parameters that influence the development of high strength, high conducting Cu-based material for pulsed magnets. It is anticipated that a correlation between the microstructure and properties of the materials will be established. Both the strength and conductivity of the materials are controlled in part by the distribution and nature of the second phase particles. It is well known that the decrease in interphase spacing results in increase in strength and a simultaneous decrease in conductivity. However, the effect of the morphology of the second phase on the properties of conductor materials is yet to be established.

The Cu-Ag was chill cast (in-house) into a 25 mm diameter cylindrical mold, while the Cu-Nb/Ti composite was supplied to us as 9.9 mm diameter rods by Oxford. Subsequent processing of the materials was carried out in-house. Briefly, the processing involved an initial swaging which resulted in converting the Cu-Ag ingots and the Cu-Nb/Ti rods to 7.7 mm diameter rods. Upon heat treating at 770 C in argon, the rods were fabricated by swaging (S), drawing (D) or by a combination of swaging and drawing (SD). The final wire diameter realized by any of these methods was 2.03 mm. The microstructure of these materials was characterized at several stages of the processing.

The microstructures of Cu-Nb/Ti composite in the as-received condition and at the conclusion of S-processing are presented in the micrographs of Figure 1a and 1b (same magnification) respectively. In both conditions, the distribution of the Nb/Ti filaments in the Cu matrix was homogeneous and remarkably uniform, which is indicative that the plastic deformation associated with this high stress deformation was very uniform. This is necessary in order to be able to optimize the property of the material. Figure 2 shows the microstructure of Cu-Ag alloy at the conclusion of S-processing. The distribution of the second phase particle (Ag) is equally homogeneous. The interparticle spacing,

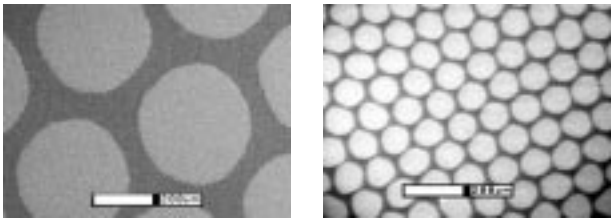

(a) (b)

Figure 1. SEM micrographs for Cu-Nb/Ti composite material (a) as received condition and (b) at the conclusion of processing.

particle size, aspect ratio of particles and volume fraction have been measured and will be used as parameters in the modeling of the effect of microstructure on strength.

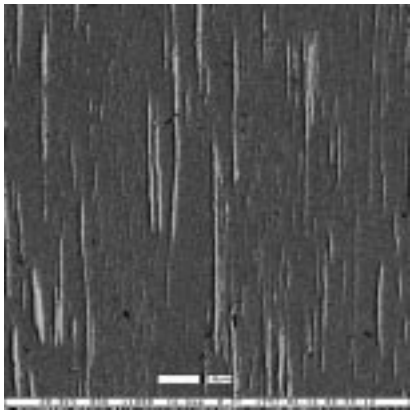

Figure 2. SEM micrograph for Cu-Ag at the conclusion of processing.

Materials Processing in Magnetic Fields: High Strength Polymers

Lincoln, D.M., UF, Materials Science Engineering
Setz, S., UF, Chemistry
Earls, J.D., The Dow Chemical Company
Priester, R.D., Jr., The Dow Chemical Company
Douglas, E.P., UF, Materials Science Engineering

Liquid crystalline thermosets (LCTs) are a new class of materials that offer a great degree of control over their properties through the modification of the molecular architecture. This can be achieved through the use of different processing and/or curing techniques. The LCT system used in this study was prepared by curing a liquid crystalline epoxy monomer, the diglycidylether of 4, 4'-dihydroxy-α-methylstilbene (DHAMS DGE), with a crosslinking agent, sulfanilamide (SAA), in a magnetic field. The system cures with smectic ordering as determined by x-ray diffraction methods. From the x-ray data two orientation parameters are calculated: the first indicating the degree of orientation of the smectic layers, and the second indicating the degree of orientation of the molecules within each layer.

Preliminary results indicate a relationship between the field strength and the orientation parameter as shown in Figure 1. One can see that the orientation parameter of the smectic layers increases with increasing field strength. These results also indicate the presence of a

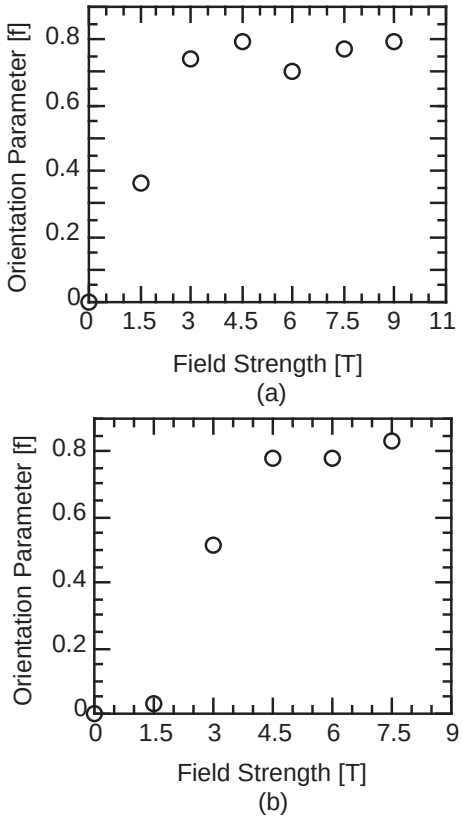

Figure 1. Orientation parameter for smectic layers as function of field strength for (a) 0 minute B-staged material, and (b) 150 minute B-staged material.

threshold field strength to impart any significant orientation in the B-staged material. However, it is not clear what the interactions are between these two factors and the time in the magnetic field.

In order to determine the interactions between the time in field, field strength, and amount of B-staging we have employed a statistical experimental design. This design involves a fractional factorial experimental design in which the three factors are varied over a specified range. Analysis of the orientation parameter data will yield the main and interaction effects of each of the factors. From this analysis we will be able to determine the value of each of the factors required to obtain a desired orientation parameter in the finished product.

Research of Composition and Cure on Epoxy for Superconducting Magnet Impregnation

Markiewicz, W.D., NHMFL
Dixon, I.R., NHMFL
Brennan, A.B., UF, Materials Science and Engineering

Introduction. Given the relation between epoxy fracture and quench, there is motivation to formulate tough epoxies for coil impregnation. One method that has previously shown effective in improving the thermal shock resistance of epoxy is the incorporation of high molecular weight components into the formulation. Following this approach, a set of compositions is prepared. The viscosity and thermal shock resistance (TSR) is examined in relation to composition and cure.

Composition Study. The effect of the substitution of increasing amounts of high molecular weight curing agent was studied in a set of three compositions, with designations NHMFL 44, NHMFL 61 (originally 44 1/2), and NHMFL 45. The high molecular weight additive (HMWA) was substituted for the primary curing agent so as to maintain an epoxy equivalent ratio of 1.0. The mixed viscosity of these compositions at 60 °C is given in Figure 1. It is seen that viscosity is not a strong function of increasing HMWA within the range of composition of these formulations. The viscosity profiles shown are considered acceptable for vacuum impregnation of large coils.

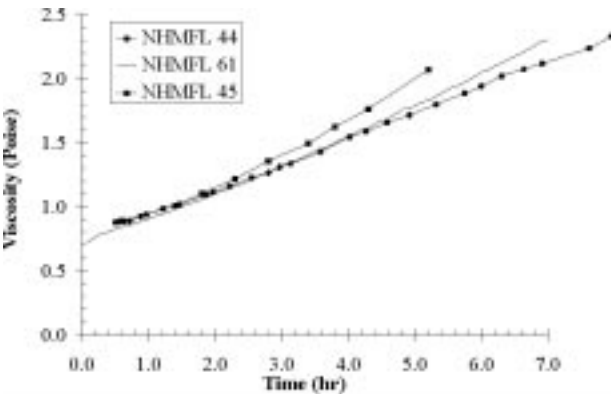

Figure 1. Viscosity profiles of NHMFL epoxies.

Cure Study. Knowing that the cure can have an influence on the TSR, two cure schedules were used. The two cure schedules have an initial temperature step of 60 °C for 24 hours and is followed by a secondary step at 80 °C for either 48 or 72 hours. The TSR samples consist of a brass bolt protruding from a short epoxy cylinder or "puck." The sample is immersed into liquid nitrogen, allowed to cool, then removed to warm to room temperature. This cycle is repeated 25 times or until failure of the sample occurs. Results of the tests are listed in Tables 1 and 2.

Table 1. Room temperature modulus and thermal shock resistance of NHMFL epoxies cured at 24 hrs/ 60 °C + 48 hrs/80 °C.

Epoxy Type	E (MPa)	% Surviving TSR Test 5 Cycles	15 Cycles	25 Cycles
NHMFL 44	1200	50	33.3	33.3
NHMFL 61	686	100	96	79
NHMFL 45	201	100	100	100

Table 2. Thermal shock resistance of NHMFL epoxies cured at 24 hrs/60 °C + 72 hrs/80 °C.

Epoxy Type	% Surviving TSR Test 5 Cycles	15 Cycles	25 Cycles
NHMFL 44	25	0	0
NHMFL 61	75	75	75
NHMFL 45	100	100	100

As the amount of HMWA increases, the glass transition temperature, T_g, is suppressed. Formulation NHMFL 61 has a T_g of essentially room temperature. Although NHMFL 44 is the most stiff, it shows a degree of TSR as a result of the HMWA content. As the HMWA is increased, the epoxy softens and the TSR improves. With additional HMWA, the epoxy softens further. There is an interest in maintaining a degree of stiffness at room temperature; thus, NHMFL 61 was selected for further cure optimization and characterization.

Microstructure, Tensile Strength, and Electrical Resistivity of a Ternary Cu-Ag-Nb MMC

Mattissen, D., IMM, RWTH Aachen, Germany
Raabe, D., Carnegie Mellon Univ., Materials Science and Engineering
Heringhaus, F., NHMFL and IMM, RWTH Aachen, Germany

The project focused on the initial experimental investigation and characterization of the ternary *in situ* metal matrix composite (MMC) Cu-8.2wt%Ag-4wt%Nb. The material was manufactured by an inductive melting technique. During the consecutive wire drawing process, the Nb and Ag phases elongated into very fine filaments. The morphology of the Ag and Nb filaments as well as the average spacing between the Ag and Nb phases were quantitatively investigated. Figure 1 shows the composite after a degree of deformation of $\eta = 4$. The Ag and Nb phases are strongly aligned parallel to the wire axis. For the quantitative analysis (Figure 2), the filaments were identified by spectra of the line scan. As a result of the fine filaments, the MMC reveals a very high tensile strength. The results of the tensile tests of the ternary MMC are given in Figure 3 in comparison with two binary MMCs.[1] The binary MMCs possess two different Nb dendrites diameters in the as-cast condition. Owing to the much smaller as-cast dendrites in the ternary MMC, this composite reaches a higher strength even with the lower volume fraction of the second phase.

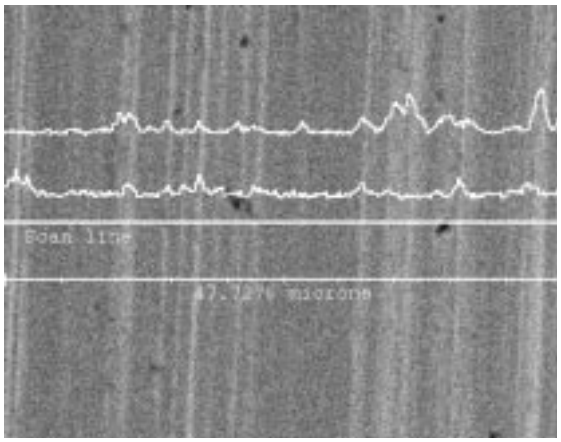

Figure 1. SEM micrograph of a Cu-Ag-Nb composite at a degree of deformation of η=4.

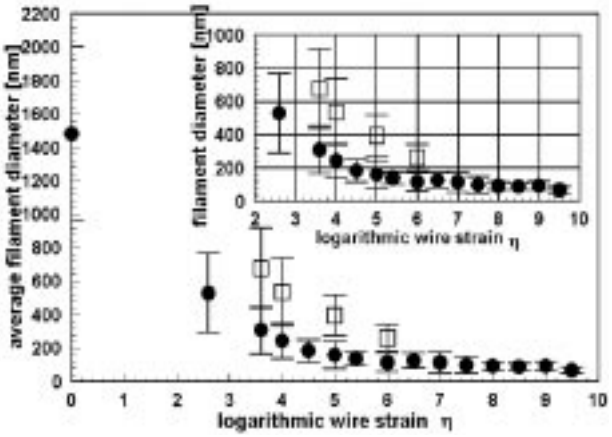

Figure 2. Average filament diameter of Nb (●) and Ag (❑) as a function of the logarithmic wire strain.

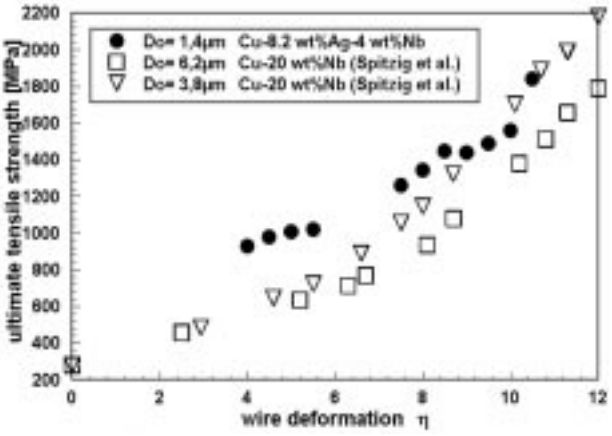

Figure 3. Ultimate tensile strength vs. wire deformation of Cu-Ag-Nb and Cu-Nb, Do=dendrite diameter in the as-cast state.

The electrical resistivity at 298 K and 77 K is given in Figure 4 as a function of the wire deformation. At a given temperature, the electrical resistivity increases with increase in wire deformation due to the refinement of the phases and the size effect. The relative changes are stronger at a lower temperature. At 4 K, the composite was found to show superconductivity although only 4.2% of its volume contain a superconductive phase.

The ternary Cu-Ag-Nb MMC, even in its non-optimized state after these initial studies, already

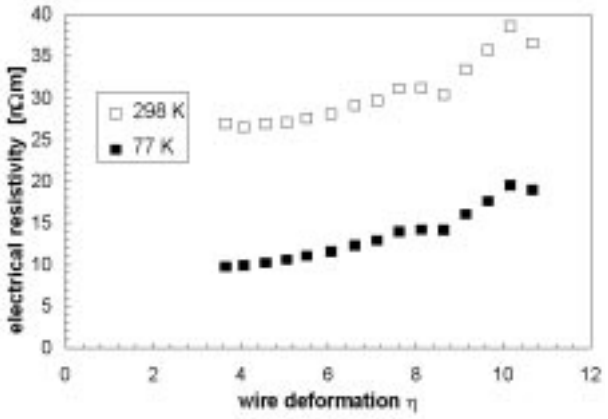

Figure 4. Electrical resistivity vs. wire deformation of Cu-Ag-Nb at 298 K and 77 K.

provides combinations of high ultimate tensile strength and a high electrical conductivity, such as 1000 MPa with 64% IACS (copper standard conductivity), 1260 MPa with 56% IACS, or 1860 MPa with 47% IACS.

References:

1 Verhoeven, J.D., *et al*., Acta Met. et Mat., 39, No. 11, 2825 (1991).

Magnetoresistivity Measurements on Various Solders for Superconducting Magnet Systems

Painter, T., NHMFL

Superconducting magnet systems often use electrical splices that require the joining of the superconductor with resistive solders. In the design of these electrical splices, it is important to know, among other things, the resistance of the solder to be used and its dependence on applied magnetic field. A proper choice of solder with lower resistivity will contribute to the decrease in electrical resistance of the splice and thereby improve the overall cryogenic performance of the superconducting magnet.

For example, in the case of the 45-T Hybrid outsert coils, it was necessary to choose a solder with a higher melting point than the traditional Sn-Pb solders due to the configuration of the electrical joint.[1] The chosen solder also had to have a sufficiently low resistivity so that the electrical heat load in the joints did not increase the load to the cryogenic system. Literature on the magnetoresistance of possible high-melting point solders, 96Sn-4Ag and 97Pb-2Ag-1Sn, did not exist, so these solders were measured.[1,2]

Subsequently, the magnetoresistivity database has been enlarged from the previously published data[1-3] by performing measurements on six types of solders as shown in Figure 1. Three of these solders have not previously been measured and will be available for future designs of electrical joints in superconducting magnets. The results show that the use of 95Sn-5Ag solder can reduce the resistance of the solder portion of the electrical splice by 48% or more in fields of 3 T or less and by 24% or more in fields of 10 T or less when compared to 50Sn-50Pb.

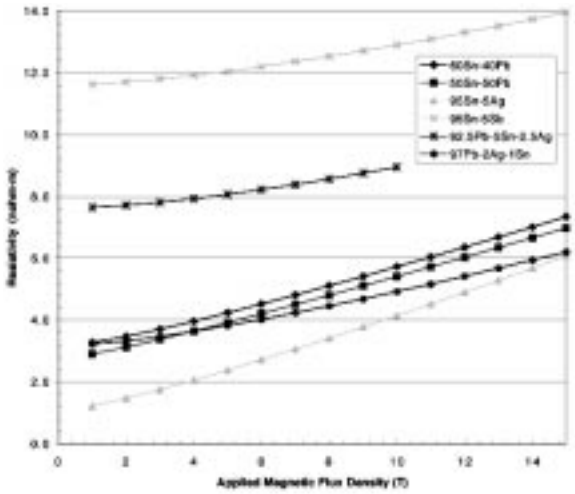

Figure 1. 95Sn-5Ag solder has a lower magnetoresistance than the standard Sn-Pb solders at all fields up to 15 T.

References:

1 Painter, T.A., *et al*., IEEE Trans. on App. Supercond., 5, 2, 753-756 (June 1995).
2 Painter, T.A., *et al*., IEEE Trans. on Magn., 30, 4, 2204-2207 (July 1994).
3 Fast, R.W., *et al*., Cryogenics, 28, 7-9 (January 1988).

New Materials for Pulse Magnets

Pernambuco-Wise, P., NHMFL
Lesch, B., NHMFL
Rickel, D., NHMFL/LANL

The NHMFL has pioneered the construction and testing of small capacitor powered pulse magnets for the evaluation of new and exotic materials destined to be used in future magnet design. The most common coils are 2 layer, 10 mm bore, copper or Glidcop conductor solenoids used to examine the behavior of outer reinforcement shells. Previous reports have detailed the results of carbon and steel shells. A new reinforcement material has recently become available in small quantities. This is a fiber produced by the TOYOBO Corporation of Japan as a non-conducting substitute for carbon fiber called Zylon. Three coils were built with varying thickness of Zylon reinforcement and tested to destruction.

The behavior of these coils is well established, over thirty have been constructed at Tallahassee, the single observation necessary is the field at which stress failure occurs. From this a direct comparison of the fiber strength with previously tested materials can be made. For each of the coils a series of 5 to 7 pulses were made. From 1 kV to 4 kV these were in increments of 1 kV, above this the increments were 500 V. The results are given in Table 1.

Table 1. Results of 10 mm material test magnets.

Magnet #	Thickness of Zylon Fiber mm	Field T
1	2	46.6
2	3	48.7
3	5	52.0

Figure 1 shows a comparison of the fiber results with those previously obtained from carbon and steel reinforcement shells. As can be seen the Zylon shells are significantly more effective than a similar thickness of carbon and comparable at least to the steel and carbon combinations. A correlation of these results with standard cryogenic tensile testing of A286 is to be performed.

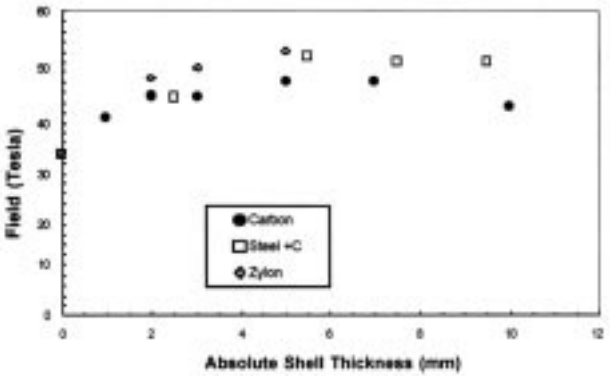

Figure 1. Comparison of the effectiveness of Zylon fiber shells with previously obtained data for carbon and A286/carbon combinations. The steel+C denotes a 2.5 mm A286 shell with additional thickness being made up with IM8 carbon fiber.

While at present only small experimental amounts of the material are available, efforts are underway to acquire a sufficient quantity to allow more elaborate testing and winding as an internal reinforcement. This is of particular importance with the CuNb/CuAg class materials where small elongation and high Young's modulus reinforcement is necessary. This fiber is likely to be superior in every way to the strongest carbon fibers even without the added advantage of being an insulator, and thus eminently suitable as internal reinforcement.

Cyclic Fatigue Behavior of Two High Strength Conductors

Walsh, R.P., NHMFL
Bednar, N.A., NHMFL
Eyssa, Y.M., NHMFL

This materials characterization program is concentrated on measuring the high cycle fatigue characteristics of CuAg and CuBe sheet materials typically used in Bitter magnet design. This research is conducted as part of an engineering design study done to provide the LANL, Manuel Lujan Jr. Neutron Scattering Center, with a 30 T split-pair

pulse magnet. The magnet operating stress and fatigue conditions, along with the electrical conductivity requirements, dictate that the conductor be a strong, fatigue resistant copper-based material such as CuBe or CuAg. The pre-existing engineering data base for these materials is insufficient for a Bitter plate design of the 30 T pulse magnet. One critical concern is the desired fatigue strength (350 - 400 MPa) of the conductor at 10^7 cycles and temperatures of around 300 K to 370 K. The characterization of the conductor materials includes 293 K static tensile tests, 293 K fatigue tests (notched and unnotched) and 393 K fatigue tests (unnotched).

The majority of the fatigue data available is for fully reverse fatigue cycling (tension/compression) where the ratio (R) of the minimum applied stress to the maximum applied stress is -1. A full reversal of stress from tension to compression is more severe than the fatigue stress regime encountered in the magnet. To simulate the service stress in the magnet the fatigue tests here were conducted in a tension/tension mode with an R = 0.1.

Due to the orthotropic nature of the CuAg material, a series of preliminary tests were conducted to evaluate the dependence of fatigue life with respect to rolling direction (RD). The results from these tests showed that samples with the tensile axis parallel to RD have inferior yield strength and fatigue strength. Therefore samples from this orientation are used throughout the remainder of the test program to provide more conservative design data.

The surface roughness of the fatigue test samples also affects the test results. One way to minimize the influence is to electropolish samples but electropolishing techniques are difficult for the CuAg material. The sheet materials have a relatively smooth surface as produced by the rolling mills (surface roughness height is less than 1E-6m). The machined edges of the samples are rougher and were sanded to an estimated surface roughness height of about 25E-6m.

The stress concentration caused by slits in the Bitter stack is complex and an exact simulation is not feasible. The effect of stress concentration is evaluated by testing samples with a circular hole at the midpoint of the gage length.

Figures 1 and 2 show the 293 K and 393 K fatigue test results for the two materials. The superior fatigue performance of the CuBe sheet is evident from the graphs. The data also show the adverse effect of a stress concentration. When the results of these tests were considered along with other design parameters, the Bitter-style design for this magnet was rejected.

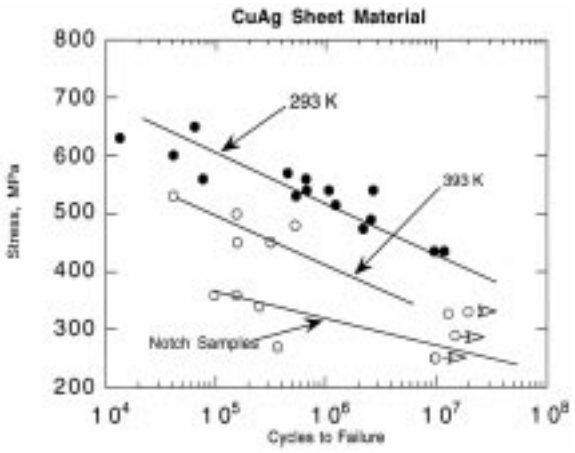

Figure 1. Test results for CuAg material.

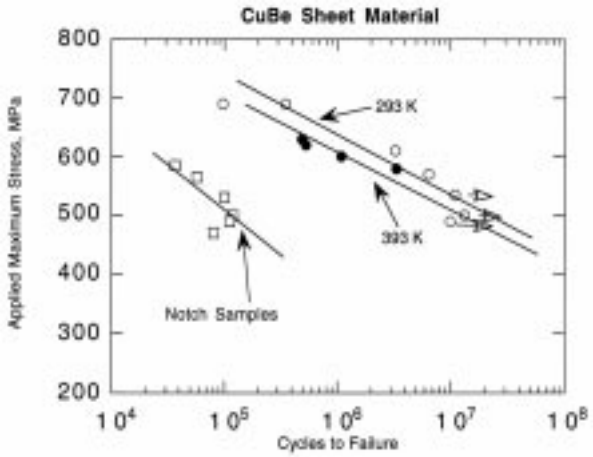

Figure 2. Test results for CuBe material.

Tests of Large-Scale Composite Supports for Superconducting Mine Countermeasure Systems

Walsh, R.P., NHMFL
Toplosky, V., NHMFL
Wendt, G., NHMFL
Creedon, W., General Atomics Inc.

The U.S. Navy Department's interest in the use of high field magnets in mine countermeasure systems has led to the development of superconducting magnet systems by General Atomics Inc. (GA). The rugged superconducting magnets could be deployed on U.S. Navy minesweeper vessels, and must be designed to operate reliably under dynamic loads up to 100 g. The high magnetic field emanated from the superconducting magnet will detonate the mines at a safe distance. Reliability of the magnet support structure is addressed here through a collaborative program between GA and NHMFL. The unique materials characterization capabilities at the NHMFL were required to provide engineers at GA with low temperature elastic properties data on prototype magnet support struts. The axial compressive modulus and Poisson ratio of sub-scale and large-scale fiber-reinforced/epoxy composite struts were determined at 295 K and 77 K at the NHMFL.

The sub-scale strut dimensions are 324 mm ID by 337 mm OD by 305 mm long. The large-scale strut dimensions are 1227 mm ID by 1251 mm OD by 559 mm long. The subscale strut was tested on the 500 kN MTS test machine shown in Figure 1. The large-scale strut test was performed on a 2.2 MN hydraulic press at the Florida Department of Transportation facilities, which is located on the same campus in close proximity to the NHMFL. Tests of the large-scale strut required the design of a large hub structure for applying a uniform axial compressive force to the 1.2 m diameter strut. A refrigeration chamber that enabled immersion of the strut in liquid nitrogen for the test was also constructed.

The properties of the struts were determined from the stress-strain curves generated during the tests. The slope of the curve for each particular gage was calculated at a value of 30 MPa (4.35 ksi) or higher (linear part of the curve) to eliminate the initial nonlinear portion of the stress-stress curve. Typical data from the gages that produced maximum and minimum slopes are plotted in Figure 2 for the large-scale strut test at 77 K. For comparison purposes, the calculated average slope is also shown on the plot.

The sub-scale strut modulus is approximately 24 GPa at 295 K increasing to 30 GPa at 77 K while the large-scale strut modulus increased from approximately 26 GPa at 295 K to 34 GPa at 77 K. Construction of the filament wound struts is essentially identical so the difference in properties are attributed to anomalies related to scaling or manufacturing. The results for the sub-scale strut are as expected while the increased stiffness observed for the large-scale strut is an unexpected benefit.

Figure 1. The sub-scale strut test.

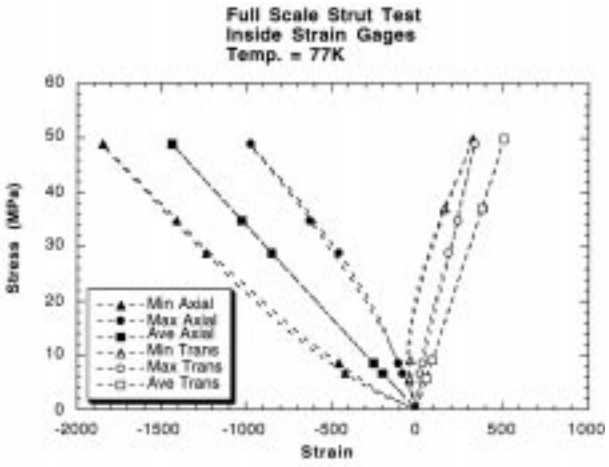

Figure 2. Typical stress-strain curve of large strut.

Thermal and Mechanical Strain Behavior of NbTi/Cu Cable Embedded in an Aluminum Stabilizer

Walsh, R.P., NHMFL
Schneider-Muntau, H.J., NHMFL
Lottin, J.C., CEA, Saclay, France

Coextrusion processing of NbTi/Cu superconducting cable inside of high purity aluminum produces a composite material with unknown and often unpredictable physical properties. Two such properties are the elastic modulus and thermal expansion. Typically the properties of a composite can be predicted using the constituent properties and the *rule of mixture* model. The properties of aluminum are well known but the cable's geometry and the effect that processing may have on the cable, complicates estimating its properties. The *in-situ* measurement method used here provides data on the composite conductor and the components. The thermal expansion from 293 K to 4 K and the 4 K elastic modulus are measured as a function of the volume fraction of superconductor cable within the composite conductor. The data are compared to properties that are estimated from simple models.

The conductor studied is a remnant from the ALEPH solenoid[1] that has a volume fraction of superconductor cable (V_{SC}) of about 0.08. Initially, tensile and thermal expansion tests of full cross-section samples are conducted. These samples are subsequently reduced in the width (approx. 50%) by machining away the aluminum conductor and then they are retested. The sample modification and retesting is repeated, allowing the same samples to be tested four times at four different superconductor to aluminum ratios. Finally the cable with no aluminum is tested to obtain the properties of the unclad cable.

The graph of elastic modulus vs. V_{SC} (Figure 1), has a line connecting the known modulus for pure aluminum to the predicted modulus of the NbTi/Cu composite. As the SC:Al ratio, increases the modulus increases in a trend similar to, but about 5 to 10% lower than the predicted data. The modulus of the pure cable (V_{SC} = 1.0) agrees well with the predicted modulus of the NbTi/Cu composite. The low modulus of the composite conductor insinuates that the NbTi cable doesn't participate equivalently in the load sharing. The cable by itself performs elastically as one would expect but when it is embedded in

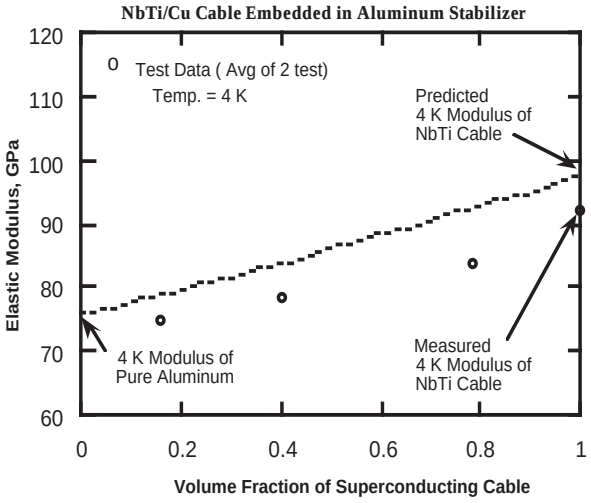

Figure 1. 4 K modulus as a function of V_{SC}.

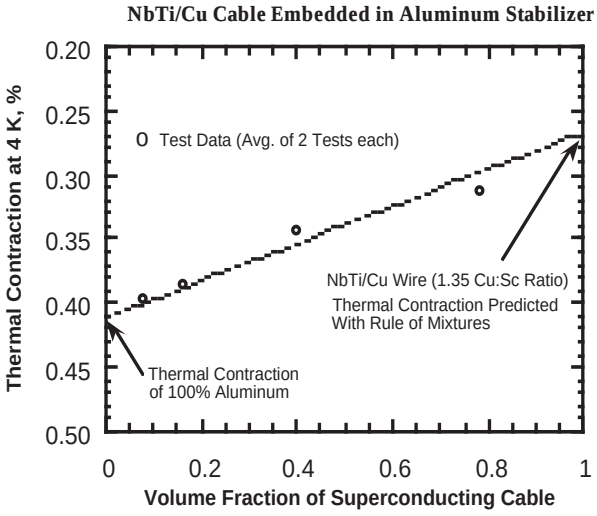

Figure 2. Thermal contraction as a function of $V_{SC.}$

the aluminum stabilizer there is a slight decrease in expected performance.

The thermal expansion test results (Figure 2) are shown as a function of V_{SC}. A line connecting the known contraction of aluminum to the predicted contraction of the NbTi/Cu composite shows that thermal expansion behaves according to the *rule of mixtures*. The thermal contraction of the materials, results in relatively low thermal stress and the two components behave in a parallel manner that can be predicted by the *rule of mixture* model.

References:

1 Le Bars, J., *et al*., IEEE Transactions on Magnetics, Mag-23, No. 2 (March 1987).